ACS Biomaterials SCIENCE & ENGINEERING

pubs.acs.org/journal/abseba

Article

Matrix Stiffness and Biochemistry Govern Colorectal Cancer Cell Growth and Signaling in User-Programmable Synthetic Hydrogels

Irina Kopyeva, Ross C. Bretherton, Jessica L. Ayers, Ming Yu, William M. Grady, and Cole A. DeForest*

Cite This: *ACS Biomater. Sci. Eng.* 2025, 11, 2810−2823

Read Online

ACCESS | Metrics & More | Article Recommendations | Supporting Information

ABSTRACT: Colorectal cancer (CRC) studies in vitro have been conducted almost exclusively on 2D cell monolayers or suspension spheroid cultures. Though these platforms have shed light on many important aspects of CRC biology, they fail to recapitulate essential cell−matrix interactions that often define in vivo function. Toward filling this knowledge gap, synthetic hydrogel biomaterials with user-programmable matrix mechanics and biochemistry have gained popularity for culturing cells in a more physiologically relevant 3D context. Here, using a poly(ethylene glycol)-based hydrogel model, we systematically assess the role of matrix stiffness and fibronectin-derived RGDS adhesive peptide presentation on CRC colony morphology and proliferation. Highlighting platform generalizability, we demonstrate that these hydrogels can support the viability and promote spontaneous spheroid or multicellular aggregate formation of six CRC cell lines that are commonly utilized in biomedical research. These gels are engineered to be fully degradable via a "biologically invisible" sortase-mediated reaction, enabling the triggered recovery of single cells and spheroids for downstream analysis. Using these platforms, we establish that substrate mechanics play a significant role in colony growth: soft conditions (∼300 Pa) encourage robust colony formation, whereas stiffer (∼2 kPa) gels severely restrict growth. Tuning the RGDS concentration did not affect the colony morphology. Additionally, we observe that epidermal growth factor receptor (EGFR) signaling in Caco-2 cells is influenced by adhesion ligand identity—whether the adhesion peptide was derived from collagen type I (DGEA) or fibronectin (RGDS)—with DGEA yielding a marked decrease in the level of downstream protein kinase phosphorylation. Taken together, this study introduces a versatile method to culture and probe CRC cell−matrix interactions within engineered 3D biomaterials.

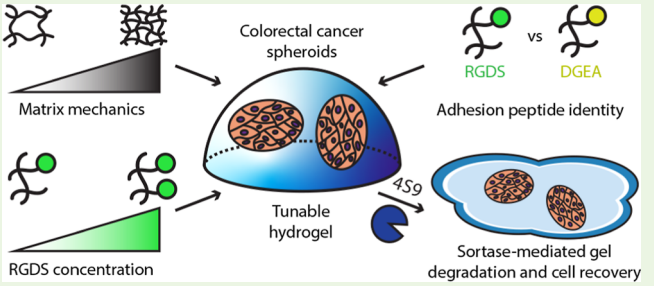

KEYWORDS: *3D hydrogel model, colorectal cancer, sortase*

INTRODUCTION

Despite advances in screening and treatment, colorectal cancer (CRC) remains the second-most prevalent cause of cancer-related death in both men and women in the United States as of 2020.[1] Currently, primary CRC tumors are typically treated successfully via surgical resection and adjuvant chemotherapy; however, metastatic CRC lesions—particularly those of the liver—continue to pose a significant challenge and thus a lower survival rate.[2] For unresectable metastatic CRC, the primary treatments are systemic administration of cytotoxic chemotherapy, targeted therapies such as antibodies for cellular receptors to growth factors, immunotherapies, and combinations thereof; however, patient response is variable, with some subsets of lesions becoming resistant.[3,4] Clinicians and researchers have begun to appreciate the role of the tumor microenvironment, a dynamic niche of various cell types and extracellular components, as a source of variability in cancer progression and drug resistance. The extracellular matrix (ECM), a protein- and sugar-rich composite surrounding cells, plays a major role in proliferation, growth, metastasis, and immune evasion in various forms of cancer, including CRC.[5−7] Building models to better understand the ECM's role in modulating cancer growth and signaling has the potential to optimize discovery phase studies for drug targets.

Over the past few decades, it has been shown that the ECM undergoes drastic biochemical, structural, and mechanical changes throughout CRC progression. Compared to healthy colonic tissue, the ECM becomes more irregular and anisotropic in CRC, with enhanced collagen deposition and cross-linking that stiffens the ECM and increases intratumoral pressure.[8] Moreover, the biochemical composition varies drastically between healthy tissue, primary tumors, and their metastases.[5] Proteomic studies on donor patients' decellularized ECM have revealed elevated levels of fibronectin in liver

Received: September 4, 2024
Revised: April 16, 2025
Accepted: April 17, 2025
Published: April 30, 2025

https://doi.org/10.1021/acsbiomaterials.4c01632
ACS Biomater. Sci. Eng. 2025, 11, 2810−2823

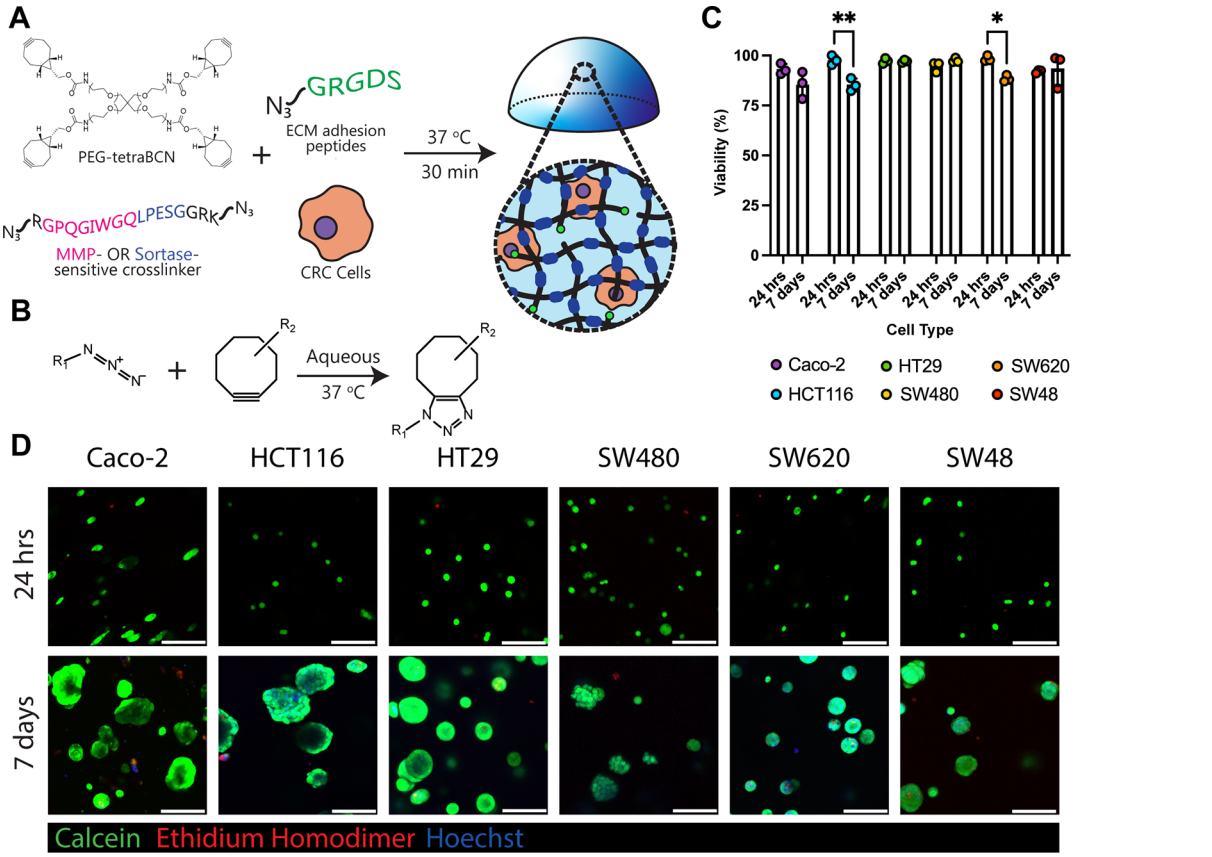

Figure 1. CRC cells are highly viable in PEG-based hydrogels. (A) Hydrogel formation proceeds spontaneously in a one-pot mixture between PEG-tetraBCN, a Boolean OR-type diazide peptide cross-linker responsive to MMP OR 4S9 Sortase, and azide-modified adhesive peptides. (B) Gel precursors are cross-linked via strain-promoted azide−alkyne cycloaddition (SPAAC) chemistry. (C) Quantification of viability of various encapsulated cell lines over 24 h and 7 days. Two-way ANOVA, Tukey's post hoc test. *$p < 0.05$; **$p < 0.01$. (D) Representative live/dead maximum image projections (MIPs). Live cells are shown in green (calcein) and dead cells in red (ethidium homodimer), with blue depicting nuclei (Hoechst). Scale bars = 100 μm.

metastases as compared to healthy tissue, findings which retrospectively correlate with worse clinical outcomes.[6,9−12]

Many biological insights have stemmed from 2D in vitro models that, while useful, do not recapitulate the in vivo microenvironments that are likely relevant for the progression of CRC. Although animal models allow researchers to study complex organ-level interactions in a 3D environment, such studies are hindered by many confounding factors and a lack of precise microenvironmental control.[13] Toward investigating the role of network biochemistry and mechanics on cancer cell signaling in vitro, researchers have implemented hydrogel biomaterials—water-swollen polymeric networks—as a tool to bridge the two models and overcome their limitations.[7,13−18] Such systems have demonstrated marked differences in drug efficacy in 2D vs 3D hydrogel models in both breast and pancreatic cancer,[19,20] implying that the 3D structure and composition of the ECM modulates drug response. Moreover, outcomes observed in these 3D models better aligned with responses in the clinic than the results from the 2D culture. However, how and why these responses occur remains largely unknown; thus, 3D biomaterial systems offer an attractive route to methodically test the impact of each independent biochemical or mechanical variable on CRC progression.

Herein, we report a synthetic poly(ethylene glycol) (PEG)-based hydrogel relying on the gentle and bioorthogonal strain-promoted azide−alkyne cycloaddition (SPAAC) between a 4-arm PEG tetrabicyclononyne (PEG-tetraBCN, which we refer to here as PEG-BCN) backbone and azide-modified peptide cross-linkers (Figure 1a,b).[21,22] We demonstrate that these hydrogels support the viability and growth of six different CRC cell lines spanning all known molecular subtypes.[23] We then utilize this system to evaluate the role of systematically tuned mechanics and integrin-binding peptide presentation in CRC morphology and proliferation. Finally, we compare how the presentation of peptide sequences for integrin binding sites of collagen I and fibronectin domains found in CRC primary and liver metastatic tumor microenvironments affects epidermal growth factor receptor (EGFR) signaling in Caco-2 cells. By customizing the gel-cross-linking peptide's sequence, the hydrogels are formulated to degrade in response to both cell-secreted matrix metalloproteinases (MMPs) and an exogenously added and "biologically invisible" sortase transpeptidase [eSrtA(4S9), which we refer to here as 4S9], serving as a Boolean OR-gated material (MMP ∨ 4S9) that enables both cell-mediated matrix remodeling and cell/spheroid recovery from gels.[22,24−27] Our group and others have recently demonstrated that sortase can be used to rapidly liberate encapsulated cells from engineered gels with minimal biological perturbations across both the transcriptome and proteome.[24,28−31] The results in this study further expand the applicability of these sortase-degradable hydrogels to a wide variety of CRC cell lines and demonstrate how tuning various hydrogel properties affects spheroid morphology, proliferation, and signaling.

https://doi.org/10.1021/acsbiomaterials.4c01632
ACS Biomater. Sci. Eng. 2025, 11, 2810−2823

MATERIALS AND METHODS

Complete experimental methods are detailed in the Supporting Information, in particular those relating to macromer/peptide synthesis and 4S9 expression and purification, which have been detailed in previous manuscripts.[24,25,30] Materials, reagents, and cell culture consumables were purchased from Sigma-Aldrich (St. Louis, MO), ThermoFisher Scientific (Waltham, MA), and ChemImpex (Wood Dale, IL), unless otherwise noted. Fmoc-protected amino acids were purchased from ChemPep (Wellington, FL).

Cell Culture. Caco-2 human colorectal adenocarcinoma cells were cultured in high-glucose Eagle's minimum essential media supplemented with 20% fetal bovine serum (FBS) and 1X penicillin−streptomycin (P/S) (Gibco, ThermoFisher; Waltham, MA). HCT116 and HT29 cells were cultured in McCoy's 5A media supplemented with 10% FBS and 1X P/S. SW480, SW620, and SW48 cells were cultured in RPMI 1640 media with 10% FBS and 1X P/S. All cells were passaged 1:10 upon reaching 80% confluency and cultured in a standard 37 °C 5% CO_2 cell culture incubator. All cell lines were obtained from ATCC and underwent DNA fingerprinting regularly to confirm their identities. The cell lines were all used at low passage number.

Live/Dead Staining. Hydrogel precursors were mixed together (final concentrations: 3 mM PEG-tetraBCN, 6 mM N_3-RGPQGIWGQLPESGGRK(N_3)-NH_2, 1 mM N_3-GRGDS-NH_2 peptides, and 1 mM N_3-GRDGS-NH_2 peptides), and cells resuspended in full-serum media were added to achieve a final concentration of 1×10^6 cells mL^{-1}. 5 μL hydrogel droplets were pipetted in the bottom of a 96-well plate and allowed to gel at 37 °C for 30 min, after which full-serum media was added to cover the gels. Cells were cultured for 24 h or 7 days, at which point gels were LIVE/DEAD-stained with calcein AM and ethidium homodimer (EtHD) (2 μM calcein and 4 μM EtHD in PBS) for 1 h. For day 7 conditions, Hoechst 33,342 (1:2000; Invitrogen; Waltham, MA) was used to obtain an accurate total cell count in colonies. Live/dead/total cell count was quantified from three 100 μm max intensity projections (MIP) per gel.

Hydrogel Rheological Characterization. Gel formation kinetics and storage moduli (G′) were analyzed on a Physica MCR-301 rheometer (Anton Paar; Graz, AT) at 37 °C with 8 mm parallel-plate geometry (0.5 mm gap, 1 Hz, 1% strain). The frequency and strain were determined to fall within the linear viscoelastic range via frequency and amplitude sweeps. Plateau moduli were estimated as the average of the final 60s of measurements. Experiments were performed in triplicate.

Cell Encapsulation for Varying RGDS and SPAAC Network Concentrations. To experimentally vary RGDS concentration, cells were encapsulated as described (3 mM PEG-BCN: 6 mM diazide cross-linker: 2 mM total pendant peptide concentration) in the Live/Dead Staining section, except with varying concentrations of N_3-GRGDS-NH_2. To achieve the same final modulus, the same total amount of pendant peptide was included in each formulation, with a sequence-scrambled peptide (N_3-GRDGS-NH_2) included to achieve 2 mM total peptide functionalization (e.g., if the concentration of RGDS was 0.5 mM, then 1.5 mM RDGS was included to yield a final concentration of 2 mM). For varying the PEG-BCN/diazide cross-linker ratio, cells were encapsulated at 2:4, 3:6, or 5:10 mM PEG-BCN/mM diazide cross-linker peptide ratios, with 1 mM RGDS included in each formulation. For all experiments, cells were encapsulated at a concentration of 1.0×10^6 cells mL^{-1} in 5 μL of hydrogel droplets on the bottom of a 96-well plate. Gels were cultured for 7 days and then fixed with 4% paraformaldehyde (PFA) for 1 h at room temperature, washed 3 × 10 min in PBS, and then incubated overnight in PBS with 0.3% Triton-X 100, Hoechst 33342 (1:2000; Invitrogen; Waltham, MA), and AlexaFluor 532-conjugated phalloidin (1:200; Life Technologies; Carlsbad, CA) overnight. The following day, gels were washed 3 × 1 h in PBS and imaged on a Leica Stellaris 5 confocal microscope. For each gel, average colony area, major axis length, and number of cells per colony were calculated from three 50 μm MIPs.

Assaying Degradation Kinetics of Hydrogels. Hydrogels were made in the following composition: 3 mM PEG-BCN/6 mM diazide. PEG-BCN was preincubated for 15 min with 50 μM AlexaFluor 568 azide (1:200 dye/PEG) (Click Chemistry Tools; Scottsdale, AZ) to fluorescently label the polymer network. Hydrogels were then formed on the bottom of a 96-well plate, either as 5 or 1 μL droplets (with the 1 μL condition having 5 gels per well)—a subset of the 5 μL droplets were smeared on the bottom of the well with a pipet tip to yield a spread-out streak—and allowed to swell overnight. The gels were washed with 1X PBS to remove any remaining unreacted dye. For testing geometry, the gels were incubated with 50 μM 4S9, 18 mM GGG, and 10 mM $CaCl_2$ (400 μL total volume). For testing 4S9 concentrations, gels were incubated with either 50, 200, or 400 μM 4S9 and 18, 72, or 144 mM GGG, respectively. The $CaCl_2$ concentration remained constant at 10 mM. To quantify the degradation extent, 2 μL of supernatant was taken from the well at each time point and diluted in 98 μL of PBS in a black 96-well plate. Fluorescent values were read on a plate reader (578/602 nm emission/excitation) (Molecular Devices; San Jose, CA) and normalized to the fluorescence values of a fully degraded gel.

Immunofluorescent Staining of Phosphorylated ERK. Caco-2 cells were encapsulated at a concentration of 1×10^6 cells mL^{-1} and cultured for 7 days. On day 6, the medium was replaced with low-serum medium (EMEM with 0.2% FBS) to starve the cells. The next day, cells were acutely treated with epidermal growth factor (EGF; 50 ng mL^{-1}; R&D Systems; Minneapolis, MN), and following the desired time point, the gels were immediately fixed with 4% paraformaldehyde in PBS for 1 h at room temperature. Gels were then washed 3 × 10 min in wash buffer [tris-buffered saline (TBS), 0.3% Triton-X 100] and blocked overnight in blocking buffer (TBS, 0.3% Triton-X 100, 1% BSA, 1% normal goat serum). Gels were incubated in primary antibody solution (wash buffer with antibody, 5% DMSO) for 24 h at RT; KI-67 antibody (#ab833; Abcam; Waltham, MA) was used at a 1:100 ratio, and pERK-p44/42 MAPK antibody (#4370; Cell Signaling Technology; Danvers, MA) was used at a 1:400 ratio. The following day, the gels were washed 3 × 2 h in wash buffer and then incubated in secondary antibody solution (wash buffer with 1:1000 IgG goat anti-rabbit AlexaFluor 647, 5% DMSO; #21244; Invitrogen; Waltham, MA) along with Hoechst 33,342 (1:2000; Invitrogen; Waltham, MA) and AlexaFluor 532-conjugated phalloidin (1:200; Life Technologies; Carlsbad, CA) overnight. The next day, gels were washed 3 × 2 h in wash buffer and imaged on a Leica Stellaris confocal microscope under 10× magnification. For each gel, average pERK fluorescence was normalized to Hoechst from three 100 μm MIPs.

Coating of 2D PDMS Surfaces. Polydimethylsiloxane (PDMS) surfaces for cell culture studies were first silanated with 5% aminopropyltriethoxysilane (APTES) in ethanol for 5 min, washed thrice each with ethanol and water, and then baked for 15 min at 80 °C to dry. After drying, plates were coated with either recombinant human fibronectin (Sigma #F2518) at a concentration of 50 μg/mL or collagen type I (Corning Inc.; Corning, NY) at a concentration of 10 μg mL^{-1}, both according to the manufacturer's instructions.[32]

Western Blotting. For 2D experiments, Caco-2 cells were seeded in coated, 6-well plates at a concentration of 1.8×10^4 cells per well. Cells were allowed to adhere and expand over 4 days, and the medium was changed every 48 h. After 4 days, cells were serum-starved overnight and the following day treated with EGF or a vehicle control for 20 min. The 6-well plates were immediately placed on ice after the 20 min treatment. The cells were washed once with ice-cold PBS and lysed on ice with a cell scraper in radioimmunoprecipitation assay (RIPA) lysis buffer containing phosphatase inhibitors and protease-inhibitor cocktail tablets.

For 3D experiments, cells were encapsulated at a concentration of 5×10^7 cells mL^{-1}, seeded in 1 μL droplets in a 48-well plate, 5 drops per well, and cultured for 5 days. As with the 2D controls, cells were serum-starved overnight on day 4. On day 5, the low-serum media was removed from the wells and replaced with 150 μL of 800 μM 4S9 solution. The gels were incubated with sortase for 45 min in a standard tissue culture incubator. After 45 min, each well was diluted

https://doi.org/10.1021/acsbiomaterials.4c01632
ACS Biomater. Sci. Eng. 2025, 11, 2810−2823

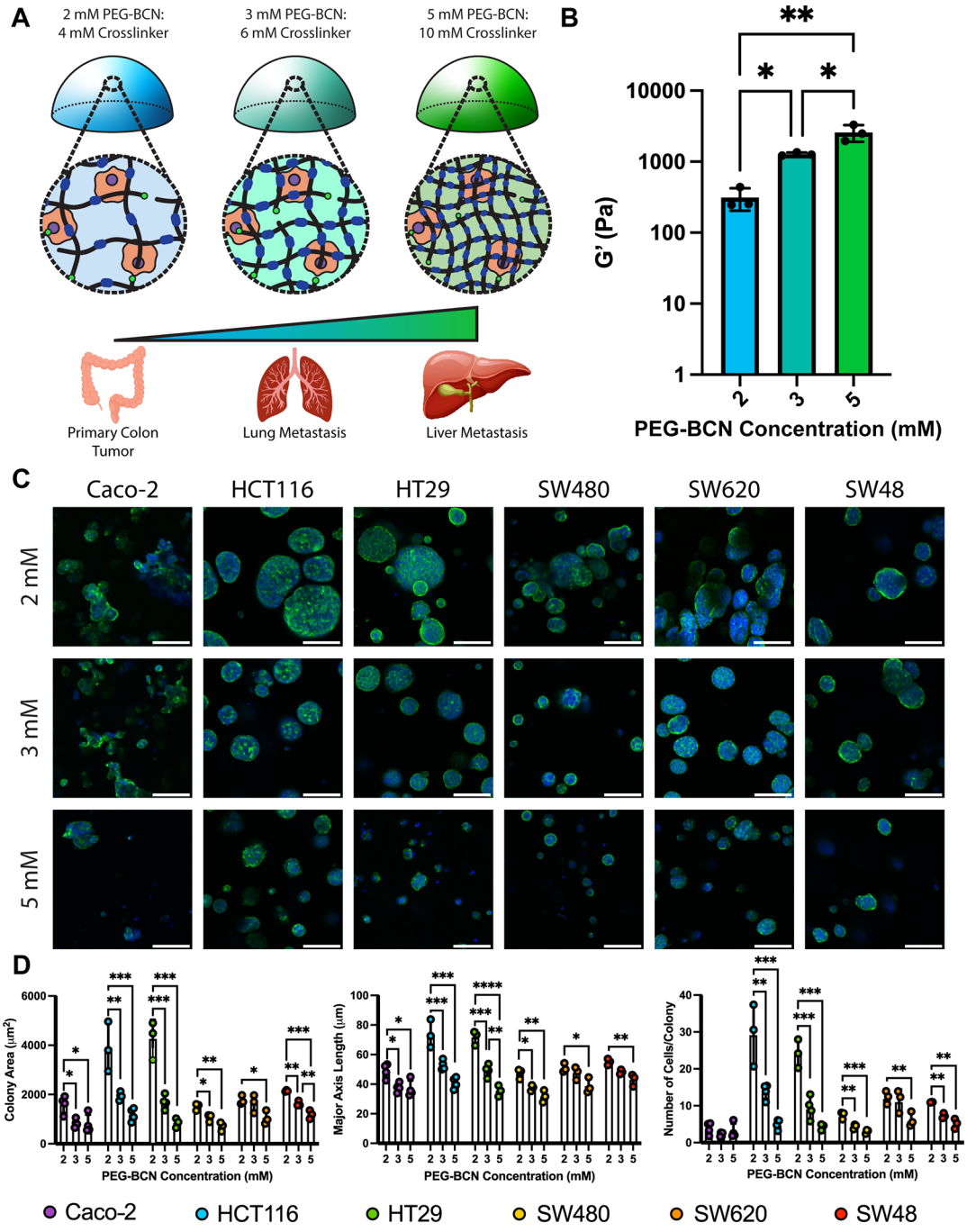

Figure 2. Effect of mechanical properties on cell line growth and colony morphology. (A) SPAAC gel precursor concentrations were varied to create gels with a range of stiffnesses that matched the range of mechanical properties encountered in primary and metastatic tumor sites. (B) Rheological characterization of SPAAC gels. One-way ANOVA, Tukey's posthoc test, *$p < 0.05$, **$p < 0.01$. (C) Representative MIPs on day 7 of various CRC cell lines cultured in gels of different stiffnesses. Shown are gels containing 2, 3, or 5 mM PEG-BCN. Scale bar = 100 μm. (D) Quantification of colony area, major axis length, and number of cells per colony as a function of gel stiffness. One-way ANOVA, Tukey's posthoc test, *$p < 0.05$, **$p < 0.01$, ***$p < 0.001$, ****$p < 0.0001$.

with 150 μL of 288 mM triglycine peptide (GGG) in low-serum media (final concentrations: 400 μM 4S9, 144 mM GGG) and treated with 50 ng mL^{-1} of EGF or vehicle control. The gels were placed back into the incubator for 20 min, during which time the hydrogels fully dissolved. The resultant cell suspensions were collected in prechilled conical tubes, pelleted at 4 °C, washed with ice-cold PBS, and resuspended in 100 μL of RIPA lysis buffer.

For both types of experiments, following resuspension in lysis buffer, cells were placed on ice and vortexed aggressively 3 × 10 min. Lysis solution was spun down at 4 °C at 14,000 rpm for 20 min to pellet cell debris. The remaining supernatant contained the extracted protein. The collected protein was quantified using a bicinchoninic acid (BCA), and Western blots were run under standard conditions looking for protein expression of phosphorylated AKT (pAKT), total AKT, phosphorylated ERK (pERK), total ERK, and GAPDH (# 9271, 4691, 4370, 4695, 8884; Cell Signaling Technology; Danvers, MA). The Western blots were imaged using the Odyssey infrared imaging system (LI-COR; Lincoln, NE) and Doc XR imaging system (Bio-Rad; Hercules, CA).

https://doi.org/10.1021/acsbiomaterials.4c01632
ACS Biomater. Sci. Eng. 2025, 11, 2810−2823

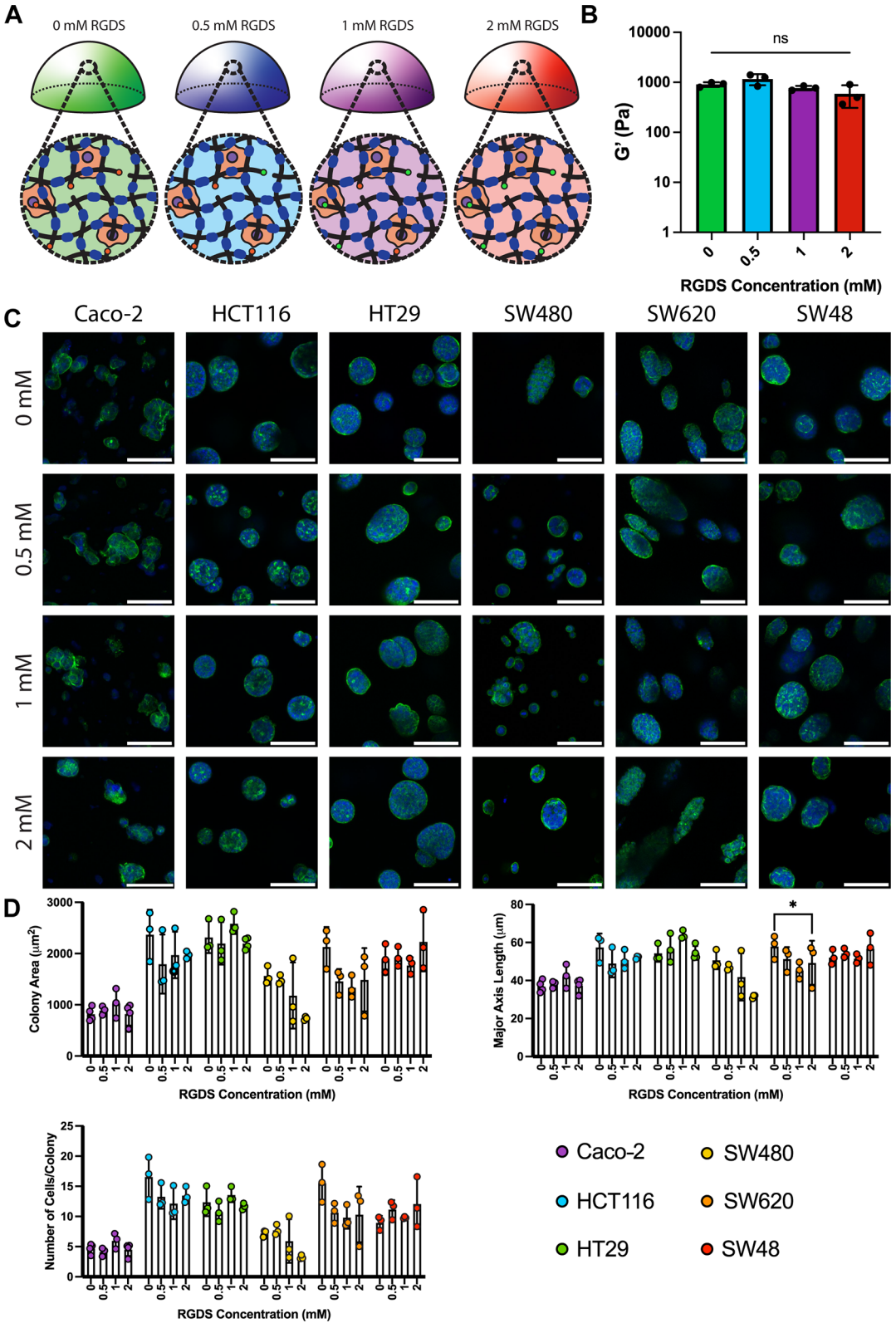

Figure 3. Effect of RGDS concentration on CRC cell line growth and colony morphology. (A) RGDS concentration was varied in the different conditions. Scrambled RGDS (RDGS) was included to keep the total peptide content constant across all conditions. (B) Rheological characterization of SPAAC gels demonstrates that matrix mechanics are unaffected by bioactive peptide content. (C) Representative MIPs on day 7 of various CRC cell lines cultured with different RGDS concentrations. Scale bar = 100 μm. (D) Quantification of colony area, major axis length, and number of cells per colony as a function of RGDS concentration. One-way ANOVA, Tukey's posthoc test, $^*p < 0.05$.

Data Analysis and Statistics. Data and statistical analysis were conducted on GraphPad Prism 7.0; the details of specific statistical methodology can be found in the figure captions. Statistical testing was conducted on a per-gel average basis as opposed to individual

https://doi.org/10.1021/acsbiomaterials.4c01632
ACS Biomater. Sci. Eng. 2025, 11, 2810−2823

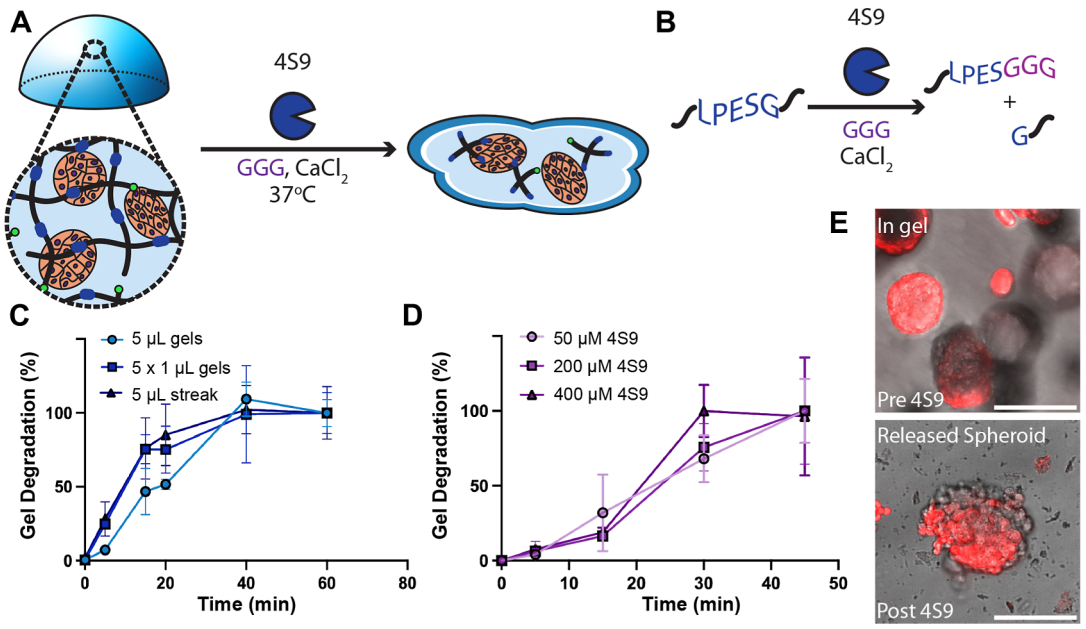

Figure 4. Sortase permits rapid and triggered degradation of cell-laden hydrogels. (A) Schematic of full gel dissolution using 4S9 to release encapsulated cells and spheroids. (B) 4S9 recognizes the sorting motif included in the peptide cross-linker to yield material degradation. (C) Gel degradation kinetics are reported as a function of gel geometry and (D) sortase concentration. Here, gels are sparsely labeled with a fluorescent dye that is released into the supernatant upon degradation and quantified via fluorescence. (E) 400 μM of 4S9 solution for 5 min allows for intact HCT116 spheroid release from gels. Prior to gel dissolution, spheroids were stained with CellTracker Red. The image represents overlaid brightfield and fluorescent channels. Scale bar = 100 μm.

cell/colony values. Fluorescent image analysis was conducted using CellProfiler v4.2.1.[33] Western blot images were analyzed using the FIJI distribution of ImageJ.[34]

RESULTS

SPAAC Hydrogels Support the Growth and Viability of Various Colon Cancer Cell Lines. To highlight our platform's broad applicability, we began by encapsulating six commonly utilized colorectal cancer cell lines in our SPAAC hydrogels. The six cell lines (Caco-2, HCT116, HT29, SW480, SW620, and SW48) were chosen for their regular use in CRC research and because they span the four distinct consensus molecular subtypes of CRC defined by differences in mutation status and tumor microenvironment.[23] Furthermore, SW480 and SW620 are two cell lines derived from the same patient, with SW480 from the primary tumor and SW620 from a metastatic lymph node site.[35] All six cell types were highly viable (>85% for all conditions) in the baseline condition of 3 mM PEG-BCN:6 mM diazide cross-linker:1 mM RGDS: 1 mM RDGS at both 24 h and 7 days (Figure 1c,d). At 24 h, cells were visibly single cells suspended in 3D; by day 7, all had grown into multicellular colonies, underscoring the prolific nature of these various cancer cell lines (Figure 1d). We observed a statistically significant drop in HCT116 and SW620 viability on day 7 with more dead cells present in the core of the spheroids, attributed to the potential difficulty of nutrient and O_2 diffusion to the core.

Gel Mechanics Influence CRC Colony Growth. As tumor microenvironment mechanics have been shown to drive the progression of various cancers, including CRC, and influence chemotherapeutic efficacy,[2,5,36,37] studies examining how culture stiffness affects CRC growth and proliferation are of vital importance. To create gels of various stiffnesses, we varied the SPAAC network molarity in our hydrogels (2:4, 3:6, or 5:10 mM PEG-BCN:mM diazide cross-linker) (Figure 2a), yielding materials that ranged from a softer 310 ± 110 Pa to the stiffer 2680 ± 680 Pa (Figure 2b). These gel stiffnesses span the range of healthy, primary, and liver metastatic tumor stiffnesses excised from patients in previous studies (G′ of primary tumors ∼100−200 Pa and G′ of liver metastases ∼1−2 kPa).[2,38] All gels formed within 20 min; however, as expected due to increased cross-linking density, the 5 mM PEG condition formed the fastest and the 2 mM PEG condition--the slowest (Supporting Information Figure S3). We encapsulated each cell line in each of the 3 variably stiff gel formulations and maintained culture for 7 days. We observed striking differences between the various SPAAC network concentrations, with cells encapsulated in the softest gels (2 mM PEG-BCN) forming large spheroids, with colonies containing upward of 30 cells per colony (Figure 2c,d). In particular, HCT116 and HT29 cell lines had large colonies (3900 ± 1010 μm^2 and 4260 ± 780 μm^2, respectively), which were significantly greater than colonies formed in the 3 and 5 mM PEG-BCN conditions, with a wide distribution of sizes (Supporting Information Figure S4a). Across all cell lines except the Caco-2s, cells in the 2 mM condition formed significantly larger and more populated colonies; in contrast, Caco-2 cells formed large colonies in the softest condition, but there was no difference in the number of cells per colony between the gel stiffness conditions. We additionally examined colony eccentricity and compactness (Supporting Information Figure S4b,c). Colony eccentricity (where a value closer to 0 signifies a more circular object, whereas closer to 1—elliptical) was significantly different between gel stiffnesses in only three cell lines (HCT116, HT29, and SW480), though the trends were different among each cell line. For HCT116, the softer gels elicited rounder colony morphologies, but stiffer gels produced colonies with rougher borders. The opposite was true for HT29 cells. SW480 cells only had a significant change

https://doi.org/10.1021/acsbiomaterials.4c01632
ACS Biomater. Sci. Eng. 2025, 11, 2810−2823

in eccentricity between 2 and 3 mM PEG conditions, potentially signifying that the intermediate stiffness promotes a more diffuse morphology, although this may not be biologically significant; interestingly, while not statistically significant, the SW620 line had a similar dip in eccentricity in the intermediate stiffness condition. Finally, colony compactness (the ratio of the area of the object to the area of a circle with the same perimeter) did not differ in a statistically significant manner between any of the conditions; across all conditions and cell types, however, compactness was greater than 1, indicating that cell proliferation was occurring at different rates throughout the spheroids.

RGDS Concentrations Do Not Affect CRC Colony Growth. After discerning the effects of matrix stiffness on CRC cell line proliferation, we asked whether varying RGDS—an adhesive peptide sequence derived from fibronectin and recognized by various integrins including $\alpha5\beta1$ and $\alpha5\beta3$[39]—ligand concentration would affect colony morphology (Figure 3a). To avoid potential variations in gel stiffness from incorporating different concentrations of pendant RGDS, all gels were formulated to contain the same total peptide content (2 mM total) with the remaining concentration filled with scrambled RDGS. Oscillatory rheology demonstrated no differences in final storage moduli and gel formation times between the various biochemical conditions (Figure 3b, Supporting Information Figure S3). Surprisingly, when the cell lines were cultured for 7 days in the varying RGDS concentrations, there were no differences in colony area or number of cells per colony, with only the SW620 cells displaying a statistical difference in the major axis length between the 0 and 2 mM RGDS conditions (Figure 3c,d).

Hydrogel Design Allows for Rapidly Triggered Biomaterial Degradation and Spheroid Recovery. While 3D culture systems are powerful for recapitulating the native tissue environment, many current models do not allow for live-cell recovery for downstream biological assays. In order to encode rapid and user-triggered degradability in our hydrogels, we turned to the bacterial transpeptidase sortase A as a "biologically invisible" tool for cell recovery from gels (Figure 4a). Wild-type sortase—a bacterial transpeptidase from *S. aureus*—recognizes the LPXTG amino acid motif and cleaves between the sorting sequence's threonine and glycine residues while covalently affixing a triglycine (GGG) motif through a native amide peptide bond (Figure 4b). Engineered sortase variants have been evolved to display improved catalytic efficiency and high substrate specificity.[40] Given the scarcity of these sortase-recognition sequences in the mammalian proteome, we and others have previously utilized this enzyme for rapid bioorthogonal dissolution and mechanical modulation of PEG-based biomaterials with no effect on the secretome.[24,28,30,41] Here, we chose to utilize the evolved sortase 4S9 variant that recognizes the LPESG peptide motif as we have previously shown that it even more minimally perturbs the mammalian transcriptome than the conventional pentamutant sortase (Figure 4b).[24] Given the requirement for extremely fast degradation and cell retrieval to study many important biological functions, including rapid phosphorylation events, we first quantified degradation rates as a function of gel geometry and 4S9/triglycine concentration. We tested three geometries: 5 μL droplets, 5 × 1 μL droplets, and 5 μL streaks smeared onto the bottom of the well plate (Figure 4c). As expected, the 5 × 1 μL droplets and 5 μL streaks degraded faster than the 5 μL droplets due to the higher surface area/volume ratios, although all had fully degraded within 40 min of treatment with 50 μM 4S9 solution. We next postulated that increasing the enzyme concentration would lead to more rapid degradation. Indeed, we saw that with the highest concentration tested (400 μM), 5 × 1 μL gels degraded within the desired time frame of 20−30 min (Figure 4d). As such, we chose to conduct our experiments that required cell release with 5 × 1 μL gels and to release cells with 400 μM 4S9 with 72 mM GGG and 1 mM $CaCl_2$ based on these results. Employing these conditions, we were able to effectively release intact HCT116 spheroids (Figure 4e).

Adhesion Ligand Identity Affects EGFR Signaling in Caco-2 Cells. While RGDS concentrations did not have a significant effect on colony morphology, biochemical composition plays a role in many signaling processes.[5] One such signaling process, the epidermal growth factor (EGF) signaling cascade, is of particular relevance for the treatment of CRC in the clinic.[42] EGFR is a transmembrane tyrosine kinase receptor protein that, like others in this family, is composed of extracellular, transmembrane, and intracellular catalytic domains. Once EGF binds EGFR, the receptor's active site is phosphorylated, which in turn initiates a variety of signaling cascades, such as the ERK/MAPK and PI3K-AKT pathways.[43] The ERK/MAPK pathway plays a major role in cell proliferation, metabolism, growth, and survival and is commonly dysregulated in many cancers including CRC.[44] Similarly, activation of the AKT pathway has been linked to cellular transformation, tumor progression, cell survival, and drug resistance as it is known to phosphorylate over 100 other proteins involved in the aforementioned cellular functions.[45] In multiple cell types, including fibroblasts and patient-derived triple-negative metastatic breast cancer cells, clustering of EGFR and fibronectin-bound integrins induces the phosphorylation of EGFR on residues different from the canonical EGF phosphorylation site, thus activating the EGFR signaling cascade in a parallel noncanonical manner. This synergy in integrin-EGFR signal transduction is thought to enhance several receptor tyrosine kinase (RTK) downstream functions, such as cell proliferation and survival, thus potentially driving EGFR-inhibitor resistance in breast cancer.[46−49]

Although several peptides have been successfully implemented to mediate cell adhesion to synthetic biomaterials, we opted to use the DGEA peptide derived from type I collagen and recognized by the $\alpha2\beta1$ integrin,[50,51] in addition to the fibronectin-mimicking RGDS. Similarly to the prior experiments, to avoid stiffness-related effects, all gels were formulated to contain the same total peptide content (2 mM total, 1 mM of each type): "RGDS gels" contained RGDS and the sequence-scrambled DGEA (sDGEA); "DGEA gels" contained DGEA and scrambled RGDS (RDGS); "RGDS + DGEA" contained both DGEA and RGDS; and negative control gels contained both scrambled DGEA and scrambled RGDS and no native peptide. Oscillatory rheology showed gel formation within 10 min, and final shear storage moduli (G′) ± standard deviation were as follows: 590 ± 60 Pa for RGD, 750 ± 320 Pa for DGEA, 760 ± 120 Pa for both, and 840 ± 110 Pa for the negative control, indicating no statistically significant effect of differing adhesion peptide sequences on gel mechanics (Supporting Information Figure S3c,d).

We chose to use Caco-2 cells for our study as they do not have *KRAS*, *BRAF*, and *NRAS* mutations, allowing for the observation of EGFR pathway regulation in response to EGF treatment.[23] After 7 days of culture, the conditions with bona

https://doi.org/10.1021/acsbiomaterials.4c01632
ACS Biomater. Sci. Eng. 2025, 11, 2810−2823

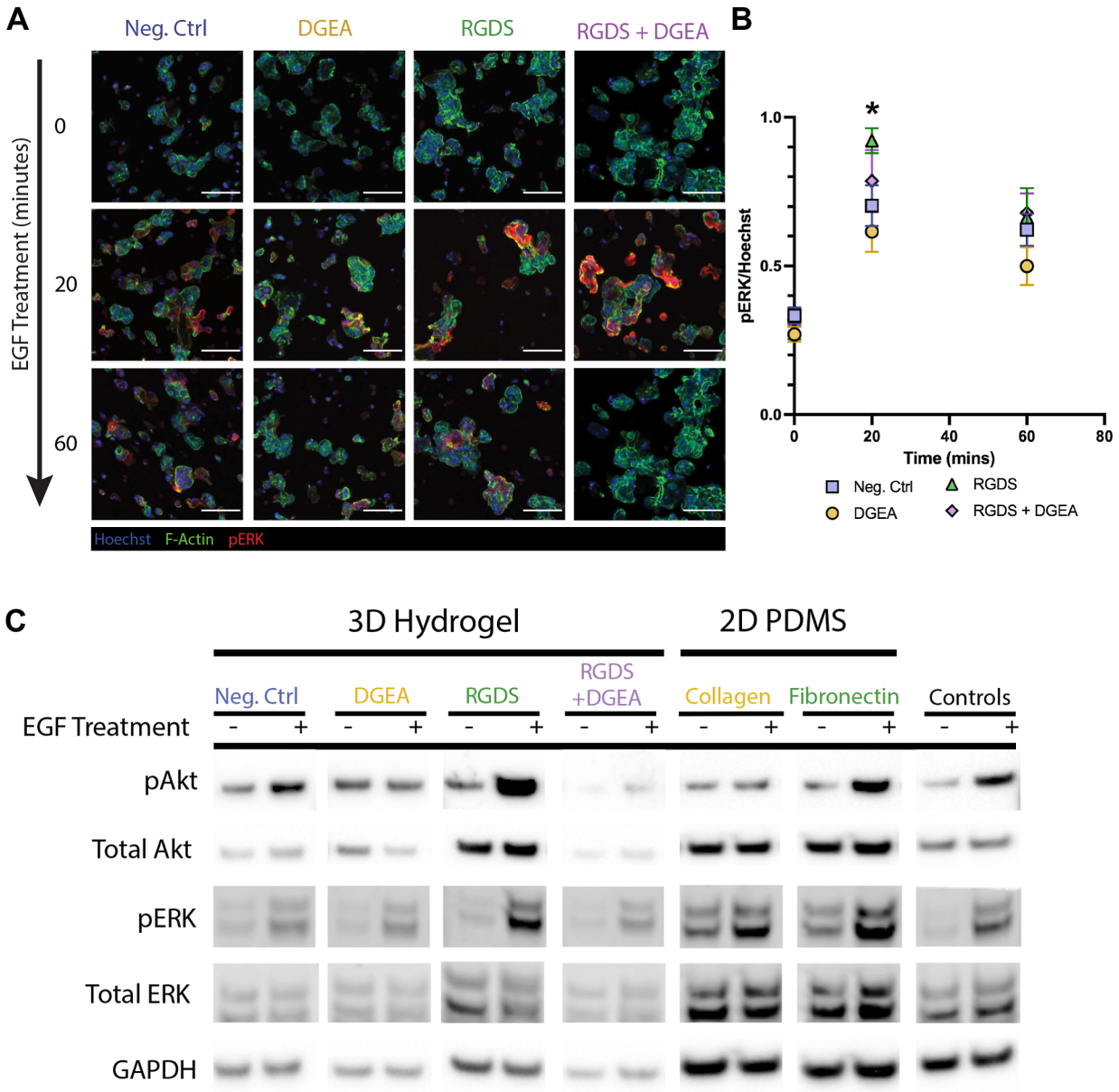

Figure 5. Matrix-bound ligand identity impacts EGFR signaling responsiveness in Caco-2 cells. (A) Caco-2 cells were encapsulated in gels of varying peptide compositions, with DGEA derived from collagen type I and RGDS from fibronectin, for 7 days and treated with EGF for 0, 20, or 60 min before fixation and immunostaining for phosphorylated ERK. Negative control conditions represent gels modified with scrambled DGEA and RGDS (DEAG and RDGS). Representative MIPs of conditions. Scale bars = 100 μm. (B) Per-gel average of the ratio of pERK/Hoechst. pERK levels spike at 20 min, with cells in DGEA-modified gels eliciting a dampened response. One-way ANOVA, Tukey's posthoc test, *$p < 0.05$. Error bars = SEM (C) Western blot for AKT and ERK from cells released from various gel formulations (left) and 2D PDMS substrates (right) shows a similar response to 3D immunofluorescence staining.

fide adhesion sequences produced large, clustered morphologies, as previously shown with Caco-2 cells in other 3D culture platforms; in contrast, the cells in negative control gels formed smaller, less diffuse clusters.[52,53] We observed that on average, colonies in the negative control gels were smaller than in the other conditions, as was expected given the lack of proper adhesion peptides. Among the three other conditions, there were no statistical differences among the colony sizes; however, DGEA gels had slightly smaller mean colony area (750 ± 140 μm^2) than RGDS (820 ± 170 μm^2) and RGDS + DGEA (780 ± 270 μm^2) (Supporting Information Figure S5c). The average number of nuclei per colony followed a similar trend, with the colonies in the negative control gels containing significantly fewer cells and DGEA gels following the same trend, again without statistical significance (Supporting Information Figure S5d). Given that serum components in media activate the EGFR pathway,[54] to eliminate this variable, we serum-starved the Caco-2 cells and assessed their proliferation by Ki-67 immunostaining. We did not observe any differences among the conditions (Supporting Information Figure S5b,e), implying that at EGF treatment time points, cells were similar in terms of basal proliferation across all formulations.

Having established that there were similar cluster morphologies among the various functional peptide-modified gel conditions, we next assessed the EGFR signaling pathway activation status to understand the effects of the microenvironment on EGF signaling. To the best of our knowledge, the

https://doi.org/10.1021/acsbiomaterials.4c01632
ACS Biomater. Sci. Eng. 2025, 11, 2810−2823

kinetics of ERK phosphorylation has not been previously assessed in a 3D in vitro culture. Caco-2 cells were cultured in gels for 6 days and serum-starved overnight. On day 7, we assessed the time dependency of ERK phosphorylation following EGF stimulation. Across all conditions, phosphorylation peaked at 20 min and decreased by 60 min (Figure 5a,b). Based on these results, we conducted the subsequent experiments with only 20 min of EGF stimulation. Cells within fibronectin-mimicking RGDS gels showed robust phosphorylation of ERK; however, strikingly, ERK phosphorylation was suppressed across all time points in gels containing DGEA and was significantly lower compared to RGDS-containing gels at 20 min ($*p < 0.05$). Interestingly, when DGEA and RGDS were both included, ERK phosphorylation was slightly increased compared to the DGEA-only condition. Cells encapsulated in negative control gels with no bona fide ECM peptides still exhibited ERK phosphorylation when treated with EGF, suggesting that EGF signaling is not solely dependent on EGFR-integrin interactions.[46] Overall, our hydrogel model was able to recapitulate EGFR signaling on similar time scales as in vivo and in 2D culture.[55−58]

Western blotting further confirmed our immunofluorescence findings: cells displayed baseline phosphorylation of ERK without EGF stimulation (Figure 5c and Supporting Information Figure S6). With EGF treatment, AKT and ERK were robustly phosphorylated under the RGDS gel conditions, a response that was suppressed in the collagen-mimicking gels (Figure 5c). We next compared the response of cells in 3D to those in 2D. Given the profound difference in stiffness between our hydrogels and tissue culture plastic that might confound results, we controlled for stiffness by coating tissue culture wells with polydimethylsiloxane (PDMS) formulated to create surfaces with $E' = 2.27 \pm 0.28$ kPa (standard deviation) by AFM (Supporting Information Figure S7). ERK and AKT phosphorylation on the PDMS surfaces followed the same trend as in 3D (Figure 5c and Supporting Information Figure S6), further bolstering our confidence in the 3D model's ability to capture the complex crosstalk of biochemical and mechanical cues in a simple, reductionist manner.

DISCUSSION

3D experimental models have become vital in the field of cancer biology for understanding the role of the ECM on tumor growth, progression, drug sensitivity, and metastasis. While in vivo rodent models remain the gold standard for studies of the tissue microenvironment, hydrogel biomaterials are promising in vitro alternatives to help bridge conventional 2D cultures and in vivo models. Currently, many laboratories employ commercially available systems such as Matrigel—solubilized basement membrane proteins extracted from a mouse sarcoma line—which, while containing the biochemical components found in the tumor stroma and supporting excellent growth of many cancer cell lines, often falls short due to its highly variable nature and its nontightly cross-linked nature (meaning elastic moduli are usually significantly softer than what would be experienced in a tumor).[59] Thus, synthetic polymeric materials present certain advantages due to their tunability: researchers can precisely control material stiffness, degradation profiles, cross-linking density, and biochemical composition, allowing for higher throughput and better controlled studies examining the effects of these variables.[60,61] Furthermore, synthetic hydrogels can be engineered with more sophisticated properties, such as the encoding of exogenously triggered degradation to allow for single-cell and even multicellular liberation from the construct.[62−64]

Previous groups have demonstrated spheroid or organoid release from synthetic hydrogels in response to shifts in temperature,[65,66] anionic exchange,[67] and 365 nm light irradiation.[68,69] These approaches have advantages and disadvantages: thermoreversible systems, while relatively easy to utilize at the bench, are not fully bioorthogonal as prolonged hyper/hypothermia may have an effect on spheroid gene expression,[70] whereas light- or anionic-based strategies may require more technical chemistry expertise to implement, which may not be readily accessible to most groups. Synthetic sortase-degradable hydrogels have been previously used by our group and others to modulate mechanics and fully degrade to release cell suspensions; these enzymatically sensitive substrate sequences can be readily inserted into virtually any peptide cross-linker.[24,28−31,41,71,72] Depending on the hydrogel assembly chemistries (e.g., Michael-type addition involving thiols natively present on cysteine side chains), these peptides can be ordered and used without further modification.[28,29,71] Recombinantly expressing sortase, while still requiring some upfront costs associated with bacterial protein expression and purification, results in high yields. Similar to previous efforts culturing cancer spheroids in sortase-degradable synthetic gels,[41,71] we newly demonstrate excellent viability of a wide variety of CRC cell lines commonly used in biomedical research in these hydrogels, two of which—SW480 and SW48—have, to the best of our knowledge, never been cultured in 3D synthetic hydrogels.

Surprisingly, as we examined the effects of matrix stiffness and ligand presentation on these cell lines, we observed that matrix stiffness had a greater effect on colony growth and morphology than the RGDS concentration. In particular, HCT116 and HT29 had the highest proliferative capacity under the softest conditions, with colony sizes far exceeding those found in the other cell types. These cell lines have been previously observed to be more proliferative in 2D cultures than SW480 and SW48. Additionally, both HCT116 and HT29 have mutations in either KRAS/BRAF or PIK3CA that yield more aggressive and proliferative phenotypes.[23] They also demonstrate aberrant DNA hypermethylation of promoter-associated CpG islands of tumor suppressor and DNA repair genes, which results in transcriptional silencing of these regulatory genes, which could also contribute to their rapid division.[73] Other cancer cell lines may not have this combination of genetic and epigenetic instabilities, leading to reduced colony size and proliferation in 3D.

The mechanical effects, while not previously systematically examined in colon cancer cell lines, could be explained by the volumetric confinement experienced by cells in a stiffer matrix: as the cells proliferate and push on the surrounding matrix, they are met with a greater resistance from the denser matrix, resulting in greater stress-induced signaling and decreased proliferation. This effect has been demonstrated in other cancer types, such as pancreatic ductal adenocarcinoma,[74,75] breast cancer,[76] hepatocarcinoma,[77] and melanoma.[78] A previous study had encapsulated a wide variety of carcinomas and shown that all of the lines proliferated the most in the soft 90 Pa fibrin gels and were more invasive compared to spheroids from stiffer cultures.[78] In a similar study, MCF-7 breast cancer spheroids grown in softer gels were more resistant to doxorubicin treatment.[76] However, these and our results do not coincide with clinical findings, where a stiffening

https://doi.org/10.1021/acsbiomaterials.4c01632
ACS Biomater. Sci. Eng. 2025, 11, 2810−2823

of the matrix accompanies malignancy.[79,80] This potentially could be explained by the tumor cells themselves cross-linking and modifying the matrix in vivo, whereas this is difficult to replicate in vitro. Additionally, hydrogel swelling and mechanical properties are difficult to disentangle, and increased swelling in a higher weight percentage gel could impart more volumetric constraint.[81] Finally, diffusion and availability of macromolecules, such as soluble growth factors and other proteins, could be decreased with increased polymer weight percentage, potentially limiting cell growth and proliferation.[82,83] Likely, the volumetric confinement coupled with the increase in concentration of protease recognition sites needed to be degraded for expansion are driving the limited colony expansion in stiffer gels.[84]

On the other hand, we observed that holding matrix mechanics constant but varying the RGDS concentration had little effect on colony morphology across all cell types; unlike cells such as hMSCs, which form more protrusions as they interact with adhesion motifs, these CRC cell lines preferentially form clusters derived from a single cell. The lack of changes in response to RGDS concentration can likely be explained by the fact that intercellular interactions within an individual cluster dominate over those with the matrix, and thus, the increased RGDS concentration is not "felt" by the majority of cells. This is slightly in contrast to other studies, such as Gjorevski et al. and Enemchukwu et al., where RGDS inclusion stimulated intestinal stem cell colony formation in a concentration-dependent manner.[85,86] On the contrary, in other studies of multicellular aggregates, such as intestinal enteroids and pancreatic cancer organoids, the inclusion of GFOGER, a collagen-derived peptide, improved organoid growth; however, the inclusion of RGDS conserved cellular viability but did not support robust organoid proliferation.[29,71]

Our findings further demonstrate that the composition of the ECM adhesion ligands, while not directly affecting cellular morphology, still impacts downstream signaling cascades. We chose to examine the modulation of the receptor tyrosine kinase EGFR, involved in proliferation, motility, cytoskeletal reorganization, and drug resistance. Strikingly, many complex aspects of ECM-EGFR cross-communication during CRC were recapitulated in this highly reductionist environment. We observed similar time scales of ERK phosphorylation and downstream signaling activation in response to acute EGF stimulation in our hydrogels as those reported in 2D monolayer cultures;[57,87−89] however, we acknowledge that fixation protocols may impact the exactness of the biological time points as paraformaldehyde diffusion into the gel is not instantaneous. We have demonstrated that adhesion with the fibronectin-binding domain synergizes with EGF stimulation to promote a robust phosphorylation response, consistent with previous results in HEK293 cells,[90] whereas association with the collagen-adhesion site dampens downstream EGFR activation, even in the presence of EGF. Previous literature in other cell types in 2D culture has shown this repressive phenotype in other cell types, such as hepatocytes and HeLa cells;[54,91,92] however, other work in Caco-2 cells has shown the opposite—in the absence of growth factors, adhesion to fibronectin did not elicit ERK phosphorylation, but adhesion to collagen type I did.[88] Yet, these 2D studies were conducted on much smaller time scales and looked at immediate adhesion to ECM molecules. In our model, over the course of a week, Caco-2 cells have presumably established more mature focal adhesions; therefore, we are able to study more reinforced, long-term interactions. In the condition that included both bioactive peptides, ERK phosphorylation was slightly increased compared to the DGEA-only condition; one potential explanation could be that the presence of the fibronectin adhesion domains allows for recruitment of fibronectin-binding integrins that supersede the signaling of collagen-binding ones. Overall, our immunostaining and Western blotting results improved our confidence that a simple 3D model could be used to interrogate complex signaling patterns in a reductionist manner.

All of the results put together, future studies looking at CRC or other cancer models should carefully consider variables such as biochemical composition and mechanical properties in their design parameters. While adhesion ligand concentration, specifically in these lines, had little effect on cell morphology, adhesion ligand identity may affect downstream signaling pathways and response to growth factor stimulation. As demonstrated here, mechanical properties could govern colony proliferation to a greater extent; therefore, future studies should consider this variable as a significant contributor to cell growth in multicellular constructs.

CONCLUSION

Herein, we present a chemically defined synthetic hydrogel model that can be utilized to systematically vary mechanical and biochemical parameters to study how these variables affect colorectal cancer growth and signaling in 3D. Through systematic variation of mechanical and biochemical parameters, we demonstrate across six CRC cell lines that mechanical properties play a much more significant role in spheroid morphology as compared with RGDS peptide concentrations. We also show that the ECM's biochemical composition has the potential to differentially modulate embedded cells' response and downstream signaling to soluble biomolecules, specifically that EGF yields differential activation of EGFR when collagen- versus fibronectin-derived peptides are present. The hydrogel system offers rapid and "biologically invisible" triggered degradability using an evolved 4S9 sortase enzyme; tuning the degradation time allowed for the recovery of full spheroids from the gels, as well as rapid cell collection for analysis of sensitive phosphorylated pathways via Western blotting. The presented methodologies are readily transferable to other hydrogel-formation chemistries and can be adopted for the higher-throughput screening of variables involved in spheroid culture.

ASSOCIATED CONTENT

Data Availability Statement

The data that support the findings of this study are available from the corresponding author upon reasonable request.

Supporting Information

The Supporting Information is available free of charge at https://pubs.acs.org/doi/10.1021/acsbiomaterials.4c01632.

Additional experimental details, materials, and methods, as well as characterization data for polymer and peptide gel precursors, sortase protein, hydrogel viscoelasticity, and cell morphology/viability analysis in gels (PDF)

AUTHOR INFORMATION

Corresponding Author

Cole A. DeForest − *Department of Bioengineering, University of Washington, Seattle 98105 Washington, United States;*

https://doi.org/10.1021/acsbiomaterials.4c01632
ACS Biomater. Sci. Eng. 2025, 11, 2810−2823

Institute of Stem Cell & Regenerative Medicine, Department of Chemical Engineering, Molecular Engineering & Sciences Institute, Department of Chemistry, and Institute for Protein Design, University of Washington, Seattle 98105 Washington, United States; orcid.org/0000-0003-0337-3577; Email: profcole@uw.edu

Authors

Irina Kopyeva − *Department of Bioengineering, University of Washington, Seattle 98105 Washington, United States; Institute of Stem Cell & Regenerative Medicine, University of Washington, Seattle 98105 Washington, United States;* orcid.org/0000-0003-3740-6971

Ross C. Bretherton − *Department of Bioengineering, University of Washington, Seattle 98105 Washington, United States; Institute of Stem Cell & Regenerative Medicine, University of Washington, Seattle 98105 Washington, United States;* orcid.org/0000-0002-9567-8556

Jessica L. Ayers − *Translational Science and Therapeutics Division, Fred Hutchinson Cancer Center, Seattle 98109 Washington, United States*

Ming Yu − *Translational Science and Therapeutics Division, Fred Hutchinson Cancer Center, Seattle 98109 Washington, United States*

William M. Grady − *Translational Science and Therapeutics Division, Fred Hutchinson Cancer Center, Seattle 98109 Washington, United States; Department of Internal Medicine, University of Washington, Seattle 98105 Washington, United States*

Complete contact information is available at: https://pubs.acs.org/10.1021/acsbiomaterials.4c01632

Author Contributions

I.K., R.C.B., J.L.A., M.Y., W.M.G., and C.A.D conceived and designed experiments. I.K. and R.C.B. executed synthesis of material precursors, protein expression, and mass spectrometry. I.K. conducted rheology. I.K. and R.C.B. conducted cell encapsulation and associated imaging experiments. R.C.B. and J.L.A. conducted fluorescent release experiments. J.L.A. conducted Western blotting experiments. I.K. and C.A.D. wrote the manuscript. M.Y., W.M.G., and C.A.D. funded experiments. M.Y., W.M.G., and C.A.D. provided mentorship and lab space.

Notes

The authors declare no competing financial interest.

■ ACKNOWLEDGMENTS

This work was supported by a Faculty Early Career Development (CAREER) Award (DMR 1652141 to C.A.D.), a standard award (DMR 1807398 to C.A.D.), and Graduate Research Fellowships (DGE 1762114 to I.K. and R.C.B.) from the National Science Foundation; a Maximizing Investigators' Research Award (R35GM138036 to C.A.D.), research grants (R01CA289291 to C.A.D. and W.M.G., R21CA283686 to C.A.D. and W.M.G., U54CA274374 to W.M.G., R50CA233042 to M.Y.), and an Interdisciplinary Training Grant (T32CA080416 to I.K.) from the National Institutes of Health. We also acknowledge the Institute for Stem Cell and Regenerative Medicine (research scholarship to R.C.B.).

■ REFERENCES

(1) Siegel, R. L.; Miller, K. D.; Goding Sauer, A.; Fedewa, S. A.; Butterly, L. F.; Anderson, J. C.; Cercek, A.; Smith, R. A.; Jemal, A. Colorectal Cancer Statistics, 2020. *CA Cancer J. Clin* **2020**, *70* (3), 145−164.

(2) Shen, Y.; Wang, X.; Lu, J.; Salfenmoser, M.; Wirsik, N. M.; Schleussner, N.; Imle, A.; Freire Valls, A.; Radhakrishnan, P.; Liang, J.; Wang, G.; Muley, T.; Schneider, M.; Ruiz de Almodovar, C.; Diz-Muñoz, A.; Schmidt, T. Reduction of Liver Metastasis Stiffness Improves Response to Bevacizumab in Metastatic Colorectal Cancer. *Cancer Cell* **2020**, *37* (6), 800−817.e7.

(3) Biller, L. H.; Schrag, D. Diagnosis and Treatment of Metastatic Colorectal Cancer: A Review. *JAMA* **2021**, *325* (7), 669−685.

(4) Misale, S.; Yaeger, R.; Hobor, S.; Scala, E.; Janakiraman, M.; Liska, D.; Valtorta, E.; Schiavo, R.; Buscarino, M.; Siravegna, G.; Bencardino, K.; Cercek, A.; Chen, C.-T.; Veronese, S.; Zanon, C.; Sartore-Bianchi, A.; Gambacorta, M.; Gallicchio, M.; Vakiani, E.; Boscaro, V.; Medico, E.; Weiser, M.; Siena, S.; Di Nicolantonio, F.; Solit, D.; Bardelli, A. Emergence of KRAS Mutations and Acquired Resistance to Anti-EGFR Therapy in Colorectal Cancer. *Nature* **2012**, *486* (7404), 532−536.

(5) Crotti, S.; Piccoli, M.; Rizzolio, F.; Giordano, A.; Nitti, D.; Agostini, M. Extracellular Matrix and Colorectal Cancer: How Surrounding Microenvironment Affects Cancer Cell Behavior? *J. Cell. Physiol.* **2017**, *232* (5), 967−975.

(6) Nyström, H. Extracellular Matrix Proteins in Metastases to the Liver - Composition, Function and Potential Applications. *Semin Cancer Biol.* **2021**, *71*, 134−142.

(7) Katz, R. R.; West, J. L. Reductionist Three-Dimensional Tumor Microenvironment Models in Synthetic Hydrogels. *Cancers (Basel)* **2022**, *14* (5), 1225.

(8) Karlsson, S.; Nyström, H. The Extracellular Matrix in Colorectal Cancer and Its Metastatic Settling - Alterations and Biological Implications. *Crit. Rev. Oncol./Hematol.* **2022**, *175*, 103712.

(9) Romero-López, M.; Trinh, A. L.; Sobrino, A.; Hatch, M. M. S.; Keating, M. T.; Fimbres, C.; Lewis, D. E.; Gershon, P. D.; Botvinick, E. L.; Digman, M.; Lowengrub, J. S.; Hughes, C. C. W. Recapitulating the Human Tumor Microenvironment: Colon Tumor-Derived Extracellular Matrix Promotes Angiogenesis and Tumor Cell Growth. *Biomaterials* **2017**, *116*, 118−129.

(10) Gulubova, M. V.; Vlaykova, T. I. Significance of Tenascin-C, Fibronectin, Laminin, Collagen IV, Alpha5beta1 and Alpha9beta1 Integrins and Fibrotic Capsule Formation around Liver Metastases Originating from Cancers of the Digestive Tract. *Neoplasma* **2006**, *53* (5), 372−383.

(11) van Huizen, N. A.; van den Braak, R. R. J. C.; Doukas, M.; Dekker, L. J. M.; IJzermans, J. N. M.; Luider, T. M. Up-Regulation of Collagen Proteins in Colorectal Liver Metastasis Compared with Normal Liver Tissue. *J. Biol. Chem.* **2019**, *294* (1), 281−289.

(12) Naba, A.; Clauser, K. R.; Whittaker, C. A.; Carr, S. A.; Tanabe, K. K.; Hynes, R. O. Extracellular Matrix Signatures of Human Primary Metastatic Colon Cancers and Their Metastases to Liver. *BMC Cancer* **2014**, *14* (1), 518.

(13) Hutmacher, D. W. Biomaterials Offer Cancer Research the Third Dimension. *Nat. Mater.* **2010**, *9* (2), 90−93.

(14) Bretherton, R. C.; DeForest, C. A. The Art of Engineering Biomimetic Cellular Microenvironments. *ACS Biomater. Sci. Eng.* **2021**, *7* (9), 3997−4008.

(15) Munoz-Robles, B. G.; Kopyeva, I.; DeForest, C. A. Surface Patterning of Hydrogel Biomaterials to Probe and Direct Cell-Matrix Interactions. *Adv. Mater. Interfaces* **2020**, *7* (21), 2001198.

(16) Nguyen, H. D.; Lin, C.-C. Viscoelastic Stiffening of Gelatin Hydrogels for Dynamic Culture of Pancreatic Cancer Spheroids. *Acta Biomater.* **2024**, *177*, 203.

(17) Gharios, R.; Francis, R. M.; DeForest, C. A. Chemical and Biological Engineering Strategies to Make and Modify Next-Generation Hydrogel Biomaterials. *Matter* **2023**, *6* (12), 4195−4244.

(18) Hassani, I.; Anbiah, B.; Moore, A. L.; Abraham, P. T.; Odeniyi, I. A.; Habbit, N. L.; Greene, M. W.; Lipke, E. A. Establishment of a Tissue-Engineered Colon Cancer Model for Comparative Analysis of Cancer Cell Lines. *J. Biomed. Mater. Res., Part A* **2024**, *112* (2), 231−249.

(19) Schwartz, A. D.; Barney, L. E.; Jansen, L. E.; Nguyen, T. V.; Hall, C. L.; Meyer, A. S.; Peyton, S. R. A Biomaterial Screening Approach Reveals Microenvironmental Mechanisms of Drug Resistance. *Integr. Biol.* **2017**, *9* (12), 912−924.
(20) Osuna de la Peña, D.; Trabulo, S. M. D.; Collin, E.; Liu, Y.; Sharma, S.; Tatari, M.; Behrens, D.; Erkan, M.; Lawlor, R. T.; Scarpa, A.; Heeschen, C.; Mata, A.; Loessner, D. Bioengineered 3D Models of Human Pancreatic Cancer Recapitulate in Vivo Tumour Biology. *Nat. Commun.* **2021**, *12* (1), 1−15.
(21) DeForest, C. A.; Polizzotti, B. D.; Anseth, K. S. Sequential Click Reactions for Synthesizing and Patterning Three-Dimensional Cell Microenvironments. *Nat. Mater.* **2009**, *8* (8), 659−664.
(22) DeForest, C. A.; Tirrell, D. A. A Photoreversible Protein-Patterning Approach for Guiding Stem Cell Fate in Three-Dimensional Gels. *Nat. Mater.* **2015**, *14* (5), 523−531.
(23) Berg, K. C. G.; Eide, P. W.; Eilertsen, I. A.; Johannessen, B.; Bruun, J.; Danielsen, S. A.; Bjørnslett, M.; Meza-Zepeda, L. A.; Eknæs, M.; Lind, G. E.; Myklebost, O.; Skotheim, R. I.; Sveen, A.; Lothe, R. A. Multi-Omics of 34 Colorectal Cancer Cell Lines - a Resource for Biomedical Studies. *Mol. Cancer* **2017**, *16* (1), 116.
(24) Bretherton, R. C.; Haack, A. J.; Kopyeva, I.; Rahman, F.; Kern, J. D.; Bugg, D.; Theberge, A. B.; Davis, J.; DeForest, C. A. User-Controlled 4D Biomaterial Degradation with Substrate-Selective Sortase Transpeptidases for Single-Cell Biology. *Adv. Mater.* **2023**, *35*, No. e2209904.
(25) Badeau, B. A.; Comerford, M. P.; Arakawa, C. K.; Shadish, J. A.; DeForest, C. A. Engineered Modular Biomaterial Logic Gates for Environmentally Triggered Therapeutic Delivery. *Nat. Chem.* **2018**, *10* (3), 251−258.
(26) Badeau, B. A.; DeForest, C. A. Programming Stimuli-Responsive Behavior into Biomaterials. *Annu. Rev. Biomed. Eng.* **2019**, *21*, 241−265.
(27) Amacher, J. F.; Antos, J. M. Sortases: Structure, Mechanism, and Implications for Protein Engineering. *Trends Biochem. Sci.* **2024**, *49* (7), 596−610.
(28) Valdez, J.; Cook, C. D.; Ahrens, C. C.; Wang, A. J.; Brown, A.; Kumar, M.; Stockdale, L.; Rothenberg, D.; Renggli, K.; Gordon, E.; Lauffenburger, D.; White, F.; Griffith, L. On-Demand Dissolution of Modular, Synthetic Extracellular Matrix Reveals Local Epithelial-Stromal Communication Networks. *Biomaterials* **2017**, *130*, 90−103.
(29) Hernandez-Gordillo, V.; Kassis, T.; Lampejo, A.; Choi, G.; Gamboa, M. E.; Gnecco, J. S.; Brown, A.; Breault, D. T.; Carrier, R.; Griffith, L. G. Fully Synthetic Matrices for *in Vitro* Culture of Primary Human Intestinal Enteroids and Endometrial Organoids. *Biomaterials* **2020**, *254*, 120125.
(30) Kopyeva, I.; Goldner, E. C.; Hoye, J. W.; Yang, S.; Regier, M. C.; Bradford, J. C.; Vera, K. R.; Bretherton, R. C.; Robinson, J. C.; DeForest, C. A. Stepwise Stiffening/Softening of and Cell Recovery from Reversibly Formulated Hydrogel Interpenetrating Networks. *Adv. Mater.* **2024**, *36*, 240880.
(31) Gilchrist, A. E.; Serrano, J. F.; Ngo, M. T.; Hrnjak, Z.; Kim, S.; Harley, B. A. C. Encapsulation of Murine Hematopoietic Stem and Progenitor Cells in a Thiol-Crosslinked Maleimide-Functionalized Gelatin Hydrogel. *Acta Biomater.* **2021**, *131*, 138−148.
(32) Teo, J.; Lim, C. T.; Yap, A. S.; Saw, T. B. A Biologist's Guide to Traction Force Microscopy Using Polydimethylsiloxane Substrate for Two-Dimensional Cell Cultures. *STAR Protocols* **2020**, *1* (2), 100098.
(33) Stirling, D. R.; Swain-Bowden, M. J.; Lucas, A. M.; Carpenter, A. E.; Cimini, B. A.; Goodman, A. CellProfiler 4: Improvements in Speed, Utility and Usability. *BMC Bioinf.* **2021**, *22* (1), 433.
(34) Schindelin, J.; Arganda-Carreras, I.; Frise, E.; Kaynig, V.; Longair, M.; Pietzsch, T.; Preibisch, S.; Rueden, C.; Saalfeld, S.; Schmid, B.; Tinevez, J.-Y.; White, D. J.; Hartenstein, V.; Eliceiri, K.; Tomancak, P.; Cardona, A. Fiji: An Open-Source Platform for Biological-Image Analysis. *Nat. Methods* **2012**, *9* (7), 676−682.
(35) Ghosh, D.; Yu, H.; Tan, X. F.; Lim, T. K.; Zubaidah, R. M.; Tan, H. T.; Chung, M. C. M.; Lin, Q. Identification of Key Players for Colorectal Cancer Metastasis by iTRAQ Quantitative Proteomics Profiling of Isogenic SW480 and SW620 Cell Lines. *J. Proteome Res.* **2011**, *10* (10), 4373−4387.
(36) Leight, J. L.; Drain, A. P.; Weaver, V. M. Extracellular Matrix Remodeling and Stiffening Modulate Tumor Phenotype and Treatment Response. *Annu. Rev. Cancer Biol.* **2017**, *1*, 313−334.
(37) Kumar, S.; Weaver, V. M. Mechanics, Malignancy, and Metastasis: The Force Journey of a Tumor Cell. *Cancer Metastasis Rev.* **2009**, *28* (1), 113−127.
(38) Pinto, M. L.; Rios, E.; Silva, A. C.; Neves, S. C.; Caires, H. R.; Pinto, A. T.; Durães, C.; Carvalho, F. A.; Cardoso, A. P.; Santos, N. C.; Barrias, C. C.; Nascimento, D. S.; Pinto-do-Ó, P.; Barbosa, M. A.; Carneiro, F.; Oliveira, M. J. Decellularized Human Colorectal Cancer Matrices Polarize Macrophages towards an Anti-Inflammatory Phenotype Promoting Cancer Cell Invasion via CCL18. *Biomaterials* **2017**, *124*, 211−224.
(39) Pierschbacher, M. D.; Ruoslahti, E. Cell Attachment Activity of Fibronectin Can Be Duplicated by Small Synthetic Fragments of the Molecule. *Nature* **1984**, *309* (5963), 30−33.
(40) Dorr, B. M.; Ham, H. O.; An, C.; Chaikof, E. L.; Liu, D. R. Reprogramming the Specificity of Sortase Enzymes. *Proc. Natl. Acad. Sci. U.S.A.* **2014**, *111* (37), 13343−13348.
(41) Arkenberg, M. R.; Moore, D. M.; Lin, C.-C. Dynamic Control of Hydrogel Crosslinking via Sortase-Mediated Reversible Transpeptidation. *Acta Biomater.* **2019**, *83*, 83−95.
(42) Kuipers, E. J.; Grady, W. M.; Lieberman, D.; Seufferlein, T.; Sung, J. J.; Boelens, P. G.; van de Velde, C. J. H.; Watanabe, T. Colorectal Cancer. *Nat. Rev. Dis. Primers* **2015**, *1*, 15065.
(43) Ponz-Sarvisé, M.; Rodríguez, J.; Viudez, A.; Chopitea, A.; Calvo, A.; García-Foncillas, J.; Gil-Bazo, I. Epidermal Growth Factor Receptor Inhibitors in Colorectal Cancer Treatment: What's New? *World J. Gastroenterol.* **2007**, *13* (44), 5877−5887.
(44) Fang, J. Y.; Richardson, B. C. The MAPK Signalling Pathways and Colorectal Cancer. *Lancet Oncol.* **2005**, *6* (5), 322−327.
(45) Matsuo, Y.; Ishihara, T.; Ishizaki, J.; Miyamoto, K.; Higaki, M.; Yamashita, N. Effect of Betamethasone Phosphate Loaded Polymeric Nanoparticles on a Murine Asthma Model. *Cell. Immunol.* **2009**, *260* (1), 33−38.
(46) Miyamoto, S.; Teramoto, H.; Gutkind, J. S.; Yamada, K. M. Integrins Can Collaborate with Growth Factors for Phosphorylation of Receptor Tyrosine Kinases and MAP Kinase Activation: Roles of Integrin Aggregation and Occupancy of Receptors. *J. Cell Biol.* **1996**, *135* (6), 1633−1642.
(47) Moro, L.; Dolce, L.; Cabodi, S.; Bergatto, E.; Erba, E. B.; Smeriglio, M.; Turco, E.; Retta, S. F.; Giuffrida, M. G.; Venturino, M.; Godovac-Zimmermann, J.; Conti, A.; Schaefer, E.; Beguinot, L.; Tacchetti, C.; Gaggini, P.; Silengo, L.; Tarone, G.; Defilippi, P. Integrin-Induced Epidermal Growth Factor (EGF) Receptor Activation Requires c-Src and p130Cas and Leads to Phosphorylation of Specific EGF Receptor Tyrosines. *J. Biol. Chem.* **2002**, *277* (11), 9405−9414.
(48) Shen, M.; Jiang, Y.-Z.; Wei, Y.; Ell, B.; Sheng, X.; Esposito, M.; Kang, J.; Hang, X.; Zheng, H.; Rowicki, M.; Zhang, L.; Shih, W. J.; Celià-Terrassa, T.; Liu, Y.; Cristea, Ii.; Shao, Z.-M.; Kang, Y. Tinagl1 Suppresses Triple-Negative Breast Cancer Progression and Metastasis by Simultaneously Inhibiting Integrin/FAK and EGFR Signaling. *Cancer Cell* **2019**, *35* (1), 64−80.e7.
(49) Bill, H. M.; Knudsen, B.; Moores, S. L.; Muthuswamy, S. K.; Rao, V. R.; Brugge, J. S.; Miranti, C. K. Epidermal Growth Factor Receptor-Dependent Regulation of Integrin-Mediated Signaling and Cell Cycle Entry in Epithelial Cells. *Mol. Cell. Biol.* **2004**, *24* (19), 8586−8599.
(50) Jha, A.; Moore, E. Collagen-Derived Peptide, DGEA, Inhibits pro-Inflammatory Macrophages in Biofunctional Hydrogels. *J. Mater. Res.* **2022**, *37* (1), 77−87.
(51) Staatz, W. D.; Fok, K. F.; Zutter, M. M.; Adams, S. P.; Rodriguez, B. A.; Santoro, S. A. Identification of a Tetrapeptide Recognition Sequence for the A2β1 Integrin in Collagen. *J. Biol. Chem.* **1991**, *266* (12), 7363−7367.

https://doi.org/10.1021/acsbiomaterials.4c01632
ACS Biomater. Sci. Eng. 2025, 11, 2810−2823

(52) Luca, A. C.; Mersch, S.; Deenen, R.; Schmidt, S.; Messner, I.; Schäfer, K. L.; Baldus, S. E.; Huckenbeck, W.; Piekorz, R. P.; Knoefel, W. T.; et al. Impact of the 3D Microenvironment on Phenotype, Gene Expression, and EGFR Inhibition of Colorectal Cancer Cell Lines. *PLoS One* **2013**, *8* (3), 59689.
(53) Dosh, R. H.; Essa, A.; Jordan-Mahy, N.; Sammon, C.; Le Maitre, C. L. Use of Hydrogel Scaffolds to Develop an in Vitro 3D Culture Model of Human Intestinal Epithelium. *Acta Biomater.* **2017**, *62*, 128−143.
(54) Mattila, E.; Pellinen, T.; Nevo, J.; Vuoriluoto, K.; Arjonen, A.; Ivaska, J. Negative Regulation of EGFR Signalling through Integrin-A1β1-Mediated Activation of Protein Tyrosine Phosphatase TCPTP. *Nat. Cell Biol.* **2005**, *7* (1), 78−85.
(55) Olsen, J. V.; Blagoev, B.; Gnad, F.; Macek, B.; Kumar, C.; Mortensen, P.; Mann, M. Global, In Vivo, and Site-Specific Phosphorylation Dynamics in Signaling Networks. *Cell* **2006**, *127* (3), 635−648.
(56) Ahmed, S.; Grant, K. G.; Edwards, L. E.; Rahman, A.; Cirit, M.; Goshe, M. B.; Haugh, J. M. Data-driven Modeling Reconciles Kinetics of ERK Phosphorylation, Localization, and Activity States. *Mol. Syst. Biol.* **2014**, *10* (1), 718.
(57) Yang, Y.-P.; Ma, H.; Starchenko, A.; Huh, W. J.; Li, W.; Hickman, F. E.; Zhang, Q.; Franklin, J. L.; Mortlock, D. P.; Fuhrmann, S.; Carter, B. D.; Ihrie, R. A.; Coffey, R. J. A Chimeric Egfr Protein Reporter Mouse Reveals Egfr Localization and Trafficking In Vivo. *Cell Rep.* **2017**, *19* (6), 1257−1267.
(58) Aoki, K.; Yamada, M.; Kunida, K.; Yasuda, S.; Matsuda, M. Processive Phosphorylation of ERK MAP Kinase in Mammalian Cells. *Proc. Natl. Acad. Sci. U.S.A.* **2011**, *108* (31), 12675−12680.
(59) Peyton, S. R.; Platt, M. O.; Cukierman, E. Challenges and Opportunities Modeling the Dynamic Tumor Matrisome. *BME Frontiers* **2023**, *4*, 0006.
(60) Liaw, C.-Y.; Ji, S.; Guvendiren, M. Engineering 3D Hydrogels for Personalized In Vitro Human Tissue Models. *Adv. Healthcare Mater.* **2018**, *7* (4), 1701165.
(61) Jonker, A. M.; Bode, S. A.; Kusters, A. H.; van Hest, J. C. M.; Löwik, D. W. P. M. Soft PEG-Hydrogels with Independently Tunable Stiffness and RGDS-Content for Cell Adhesion Studies. *Macromol. Biosci.* **2015**, *15* (10), 1338−1347.
(62) Peyton, S. R.; Chow, L. W.; Finley, S. D.; Versypt, A. N. F.; Hill, R.; Kemp, M. L.; Langer, E. M.; McGuigan, A. P.; Meyer, A. S.; Seidlits, S. K.; Roy, K.; Mumenthaler, S. M. Synthetic Living Materials in Cancer Biology. *Nat. Rev. Bioeng.* **2023**, *1* (12), 972−988.
(63) Rapp, T. L.; DeForest, C. A. Visible Light-Responsive Dynamic Biomaterials: Going Deeper and Triggering More. *Adv. Healthc. Mater.* **2020**, *9* (7), 1901553.
(64) Li, Y.; Kumacheva, E. Hydrogel Microenvironments for Cancer Spheroid Growth and Drug Screening. *Sci. Adv.* **2018**, *4* (4), No. eaas8998.
(65) Li, Y.; Khuu, N.; Gevorkian, A.; Sarjinsky, S.; Therien-Aubin, H.; Wang, Y.; Cho, S.; Kumacheva, E. Supramolecular Nanofibrillar Thermoreversible Hydrogel for Growth and Release of Cancer Spheroids. *Angew. Chem., Int. Ed.* **2017**, *56* (22), 6083−6087.
(66) Saravanou, S. F.; Ioannidis, K.; Dimopoulos, A.; Paxinou, A.; Kounelaki, F.; Varsami, S. M.; Tsitsilianis, C.; Papantoniou, I.; Pasparakis, G. Dually Crosslinked Injectable Alginate-Based Graft Copolymer Thermoresponsive Hydrogels as 3D Printing Bioinks for Cell Spheroid Growth and Release. *Carbohydr. Polym.* **2023**, *312*, 120790.
(67) Hai, J.; Zeng, X.; Zhu, Y.; Wang, B. Anions Reversibly Responsive Luminescent Nanocellulose Hydrogels for Cancer Spheroids Culture and Release. *Biomaterials* **2019**, *194*, 161−170.
(68) Yavitt, F. M.; Brown, T. E.; Hushka, E. A.; Brown, M. E.; Gjorevski, N.; Dempsey, P. J.; Lutolf, M. P.; Anseth, K. S. The Effect of Thiol Structure on Allyl Sulfide Photodegradable Hydrogels and Their Application as a Degradable Scaffold for Organoid Passaging. *Adv. Mater.* **2020**, *32* (30), 1905366.
(69) Kopyeva, I.; Brady, R. P.; DeForest, C. A. Light-Based Fabrication and 4D Customization of Hydrogel Biomaterials. *Nat. Rev. Bioeng* **2024**, *3*, 159−180.
(70) Sonna, L. A.; Fujita, J.; Gaffin, S. L.; Lilly, C. M. Invited review: Effects of heat and cold stress on mammalian gene expression. *J. Appl. Physiol.* **2002**, *92* (4), 1725−1742.
(71) Below, C. R.; Kelly, J.; Brown, A.; Humphries, J. D.; Hutton, C.; Xu, J.; Lee, B. Y.; Cintas, C.; Zhang, X.; Hernandez-Gordillo, V.; Stockdale, L.; Goldsworthy, M. A.; Geraghty, J.; Foster, L.; O'Reilly, D. A.; Schedding, B.; Askari, J.; Burns, J.; Hodson, N.; Smith, D. L.; Lally, C.; Ashton, G.; Knight, D.; Mironov, A.; Banyard, A.; Eble, J. A.; Morton, J. P.; Humphries, M. J.; Griffith, L. G.; Jørgensen, C. A Microenvironment-Inspired Synthetic Three-Dimensional Model for Pancreatic Ductal Adenocarcinoma Organoids. *Nat. Mater.* **2022**, *21* (1), 110−119.
(72) Haack, A. J.; Brown, L. G.; Goldstein, A. J.; Mulimani, P.; Berthier, J.; Viswanathan, A. R.; Kopyeva, I.; Whitten, J. M.; Lin, A.; Nguyen, S. H.; Leahy, T. P.; Bouker, E. E.; Padgett, R. M.; Mazzawi, N. A.; Tokihiro, J. C.; Bretheron, R. C.; Wu, A.; Tapscott, S. J.; DeForest, C. A.; Popowics, T. E.; Berthier, E.; Sniadecki, N. J.; Theberge, A. B. Suspended Tissue Open Microfluidic Patterning (STOMP). *Adv. Sci.* **2025**, 2501148.
(73) Ahmed, D.; Eide, P. W.; Eilertsen, I. A.; Danielsen, S. A.; Eknæs, M.; Hektoen, M.; Lind, G. E.; Lothe, R. A. Epigenetic and Genetic Features of 24 Colon Cancer Cell Lines. *Oncogenesis* **2013**, *2* (9), No. e71.
(74) Liu, H.-Y.; Korc, M.; Lin, C.-C. Biomimetic and Enzyme-Responsive Dynamic Hydrogels for Studying Cell-Matrix Interactions in Pancreatic Ductal Adenocarcinoma. *Biomaterials* **2018**, *160*, 24−36.
(75) Arkenberg, M. R.; Lin, C.-C. Orthogonal Enzymatic Reactions for Rapid Crosslinking and Dynamic Tuning of PEG-Peptide Hydrogels. *Biomater. Sci.* **2017**, *5* (11), 2231−2240.
(76) Li, Y.; Khuu, N.; Prince, E.; Tao, H.; Zhang, N.; Chen, Z.; Gevorkian, A.; McGuigan, A. P.; Kumacheva, E. Matrix Stiffness-Regulated Growth of Breast Tumor Spheroids and Their Response to Chemotherapy. *Biomacromolecules* **2021**, *22* (2), 419−429.
(77) Liang, Y.; Jeong, J.; DeVolder, R. J.; Cha, C.; Wang, F.; Tong, Y. W.; Kong, H. A Cell-Instructive Hydrogel to Regulate Malignancy of 3D Tumor Spheroids with Matrix Rigidity. *Biomaterials* **2011**, *32* (35), 9308−9315.
(78) Liu, J.; Tan, Y.; Zhang, H.; Zhang, Y.; Xu, P.; Chen, J.; Poh, Y.-C.; Tang, K.; Wang, N.; Huang, B. Soft Fibrin Gels Promote Selection and Growth of Tumorigenic Cells. *Nat. Mater.* **2012**, *11* (8), 734−741.
(79) Lampi, M. C.; Reinhart-King, C. A. Targeting Extracellular Matrix Stiffness to Attenuate Disease: From Molecular Mechanisms to Clinical Trials. *Sci. Transl. Med.* **2018**, *10* (422), 475.
(80) Levental, K. R.; Yu, H.; Kass, L.; Lakins, J. N.; Egeblad, M.; Erler, J. T.; Fong, S. F. T.; Csiszar, K.; Giaccia, A.; Weninger, W.; Yamauchi, M.; Gasser, D. L.; Weaver, V. M. Matrix Crosslinking Forces Tumor Progression by Enhancing Integrin Signaling. *Cell* **2009**, *139* (5), 891−906.
(81) Long, H.; Vos, B. E.; Betz, T.; Baker, B. M.; Trappmann, B. Nonswelling and Hydrolytically Stable Hydrogels Uncover Cellular Mechanosensing in 3D. *Adv. Sci.* **2022**, *9* (12), 2105325.
(82) Richbourg, N. R.; Peppas, N. A. Solute Diffusion and Partitioning in Multi-Arm Poly(Ethylene Glycol) Hydrogels. *J. Mater. Chem. B* **2023**, *11* (2), 377−388.
(83) Lee, S.; Tong, X.; Yang, F. The Effects of Varying Poly(Ethylene Glycol) Hydrogel Crosslinking Density and the Crosslinking Mechanism on Protein Accumulation in Three-Dimensional Hydrogels. *Acta Biomater.* **2014**, *10* (10), 4167−4174.
(84) Brown, A.; He, H.; Trumper, E.; Valdez, J.; Hammond, P.; Griffith, L. G. Engineering PEG-Based Hydrogels to Foster Efficient Endothelial Network Formation in Free-Swelling and Confined Microenvironments. *Biomaterials* **2020**, *243*, 119921.
(85) Gjorevski, N.; Sachs, N.; Manfrin, A.; Giger, S.; Bragina, M. E.; Ordóñez-Morán, P.; Clevers, H.; Lutolf, M. P. Designer Matrices for

Intestinal Stem Cell and Organoid Culture. *Nature* **2016**, *539* (7630), 560−564.
(86) Enemchukwu, N. O.; Cruz-Acuña, R.; Bongiorno, T.; Johnson, C. T.; García, J. R.; Sulchek, T.; García, A. J. Synthetic Matrices Reveal Contributions of ECM Biophysical and Biochemical Properties to Epithelial Morphogenesis. *J. Cell Biol.* **2016**, *212* (1), 113−124.
(87) Pinilla-Macua, I.; Grassart, A.; Duvvuri, U.; Watkins, S. C.; Sorkin, A. EGF Receptor Signaling, Phosphorylation, Ubiquitylation and Endocytosis in Tumors in Vivo. *eLife* **2017**, *6*, No. e31993.
(88) Sanders, M. A.; Basson, M. D. Collagen IV-Dependent ERK Activation in Human Caco-2 Intestinal Epithelial Cells Requires Focal Adhesion Kinase. *J. Biol. Chem.* **2000**, *275* (48), 38040−38047.
(89) Kiyatkin, A.; van Alderwerelt van Rosenburgh, I. K.; Klein, D. E.; Lemmon, M. A. Kinetics of Receptor Tyrosine Kinase Activation Define ERK Signaling Dynamics. *Sci. Signal.* **2020**, *13* (645), No. eaaz5267.
(90) Yarwood, S. J.; Woodgett, J. R. Extracellular Matrix Composition Determines the Transcriptional Response to Epidermal Growth Factor Receptor Activation. *Proc. Natl. Acad. Sci. U.S.A.* **2001**, *98* (8), 4472−4477.
(91) Fassett, J. T.; Tobolt, D.; Nelsen, C. J.; Albrecht, J. H.; Hansen, L. K. The Role of Collagen Structure in Mitogen Stimulation of ERK, Cyclin D1 Expression, and G1-S Progression in Rat Hepatocytes. *J. Biol. Chem.* **2003**, *278* (34), 31691−31700.
(92) Mehta, M.; Madl, C. M.; Lee, S.; Duda, G. N.; Mooney, D. J. The Collagen I Mimetic Peptide DGEA Enhances an Osteogenic Phenotype in Mesenchymal Stem Cells When Presented from Cell-Encapsulating Hydrogels. *J. Biomed. Mater. Res. A* **2015**, *103* (11), 3516−3525.

https://doi.org/10.1021/acsbiomaterials.4c01632
ACS Biomater. Sci. Eng. 2025, 11, 2810−2823